Received: 5 January 2022 | Revised: 11 April 2022 | Accepted: 14 April 2022

DOI: 10.1002/cjce.24593

RESEARCH ARTICLE

THE CANADIAN JOURNAL OF CHEMICAL ENGINEERING

Kinetic and mechanistic aspects of furfural degradation in biorefineries

Lukas Almhofer[1,2] | **Robert H. Bischof**[3] | **Martin Madera**[3] | **Christian Paulik**[2]

[1]Wood K plus–Competence Center for Wood Composites & Wood Chemistry, Kompetenzzentrum Holz GmbH, Linz, Austria

[2]Institute for Chemical Technology of Organic Materials, Johannes Kepler University Linz, Linz, Austria

[3]Lenzing AG, Lenzing, Austria

Correspondence
Lukas Almhofer, Wood K plus–Competence Center for Wood Composites & Wood Chemistry, Kompetenzzentrum Holz GmbH, Linz, 4040, Austria.
Email: l.almhofer@wood-kplus.at

Funding information
Austrian Research Promotion Agency (FFG), Grant/Award Number: 844608

Abstract

Furfural is one of the most promising platform chemicals for a future biobased industry and can already be produced from renewable raw materials. However, its production processes suffer from yield loss and fouling problems due to degradation reactions. To increase our understanding of furfural stability, we investigated the kinetics of its degradation (i) without acid catalyst and (ii) in 10 different acids that are frequently used in biomass processing or that are naturally present in biomass hydrolysates. The batch experiments were conducted in a parallel minireactor setup at temperatures ranging from 125 to 200°C. The results showed that acid-catalyzed furfural degradation reactions depend mainly on acid strength and give rise to a set of common degradation products (formic acid, glycolic acid, pyruvate, etc.). Sulphurous acid and lignosulphonic acid led to greater furfural degradation than expected, which appears to be driven by specific side reactions. Adding formic acid, in contrast, led to a lower degradation rate than expected. In general, we observed two distinct, competing degradation mechanisms. Selectivity for formic acid as a degradation product depends on temperature, furfural concentration, and the presence of an acid catalyst. A more detailed study of the formic acid yielding reaction showed it to be reversible, and we provide the first quantitative description of this reaction for any furan. The proposed kinetic model, together with the results presented, contributes to the development of more efficient furfural production processes.

KEYWORDS

acid catalysis, electron microscopy, formic acid, infrared spectroscopy, kinetic modelling

1 | INTRODUCTION

Realizing more sustainable economic development in the 21st century requires the production of materials, chemicals, and fuels to shift towards using bio-based raw materials.[1] The uncertain availability of fossil resources, their considerable price fluctuations, and the emission of carbon dioxide and other greenhouse gases are the main reasons why existing value chains must be replaced with more ecologically benign alternatives. Biorefineries use

abundantly available biomass as feedstock for the supply of so-called the biobased platform molecules and represent a promising concept for a future bio-based (chemical) industry.

Furfural, which can be derived from xylans, abundantly available in the lignocellulose of hardwoods or perennial plants such as wheat and corn, has previously been identified as a promising platform molecule for biobased aromatics.[2,3] It is currently used as a solvent, wetting agent, and as a key derivative for producing other chemicals like levulinic acid,[4] γ-valerolactone,[5] and 2-methylfuran.[6] The majority of furfural is reduced to furfuryl alcohol, which serves as a monomer in the synthesis of furan resins; however, over 80 different molecules could, in theory, be synthesized starting from furfural.[7]

Commercial production of furfural started in 1922 by acidic digestion of oat hulls, and today's processes continue to be based largely on the same principle. Feedstocks with high pentose or pentosan contents are heated to temperatures between 150 and 200°C under acidic conditions, and furfural forms through multiple dehydration steps from xylose. Industrial continuous steam stripping processes typically have yields of less than 60%, and even several improved technologies do not come close to theoretical yields.[8,9] Furfural has multiple functional groups, and thus various side reactions, like electrophilic substitutions, aldol, or Diels–Alder reactions, can occur and lower process efficiency. Reactions between furfural and xylose or intermediates in the dehydration of xylose are considered to be the main causes of low yields.[9] To overcome this problem, a variety of approaches have sought to separate furfural from the reaction medium in situ, for instance, by acidic steam stripping,[10] extraction with inert solvents,[11–13] or using ionic liquids.[14]

Even if reactions with other species are successfully prevented, furfural may form solid by-products by degradation or self-polymerization reactions. These solids, called humins, lead to complications—not only during the formation but also in the isolation and purification of furfural. Though the kinetics and mechanistic aspects of the furfural formation reaction and its side reactions have recently been investigated,[15–17] furfural degradation has received less attention.[18,19] For the furfural derivative 5-hydroxymethylfurfural (HMF), the degradation pathways were examined in more detail, and several studies analyzing HMF-derived humins were published.[20–22] A range of reaction mechanisms, such as electrophilic substitutions,[23] Diels–Alder reactions,[16] and aldol reactions[24] were proposed. Shi and coworkers[25] suggested that the formation of α-carbonyl aldehydes by hydrolytic cleavage of the furan ring is responsible for the formation of humins in subsequent condensation reactions. However, it remains unclear which of these mechanisms is the main cause for the formation of humins and whether these findings can be transferred to furfural. Besides these solid substances, formic acid has been reported as a product of furfural degradation, but to the best of our knowledge, its formation has not been quantified and investigated in detail so far.

It is known that furfural is not stable in aqueous solutions, especially at high temperatures and under acidic conditions.[26] Most of the research into furfural degradation has been conducted in aqueous solutions of sulphuric[11,27] or hydrochloric acid.[16,19] Only a few results have been published about the effects of other acids, for example, organic or multivalent acids,[18,28–30] even though several organic acids are present in biomass hydrolysate and could influence the degradation behaviour of furfural. Furthermore, acids like acetic or formic acid are by-products of biorefineries or pulp and paper mills and could thus be used as more ecologically benign alternatives to sulphuric or hydrochloric acid. In this paper, we present the first detailed investigation of the influence on furfural reactivity of 10 selected acids relevant for biorefinery processes. Our results support research into improved catalysts for furfural production and clarify how acids originating from biomass affect the production process of furfural and the formation of humin-like by-products. We propose a novel kinetic model of the degradation of furfural which—together with an analysis of the reaction products—offers insights into possible reaction mechanisms and increases our understanding of the degradation pathways of furfural. The present study helps to expand the understanding of furfural degradation in biorefineries by elucidating the effect of reaction conditions and organic acids on furfural degradation. Emphasis is also placed on the role of formic acid during furfural degradation, and our study shows that switching to formic acid as a catalyst for furfural production can reduce the formation of undesirable humin by-products.

2 | EXPERIMENTAL SECTION

2.1 | Chemicals

The acids that were investigated for their influence on furfural degradation at 150°C, including purity, supplier, molecular formula, and acid dissociation constants, can be found in Table 1. Furfural was provided by Lenzing AG from the top of a furfural purification column with 99.5% purity and stored under an argon atmosphere in a refrigerator. Unless otherwise specified, all other chemicals were of analytical grade, obtained from commercial suppliers, and used without further purification.

TABLE 1 Acids investigated for their influence on furfural degradation at 150°C, including their corresponding abbreviations, purities, suppliers, Chemical Abstracts Service Registry Number (CAS Reg. No.), molecular formulas, and calculated acid dissociation constants at 150°C

Name	Abbreviation	Purity (g/g)	Supplier	CAS Reg. No.	Molecular formula	pK_A at 150°C
Propionic acid	PA	>0.995	Fluka	79-09-4	$C_3H_6O_2$	5.30[31]
Acetic acid	AA	p.a.	Sigma-Aldrich	64-19-7	$C_2H_4O_2$	5.18[32]
Succinic acid	SA	0.999	VWR	110-15-6	$C_4H_6O_4$	4.53[a][33]
Formic acid	FA	0.88–0.91	Fluka	64-18-6	CH_2O_2	4.20[18]
Citric acid anhydrous	CA	≥0.995	Fluka	77-92-9	$C_6H_8O_7$	3.34[34] 5.24[34] 7.40[34]
Disodium hydrogen citrate sesquihydrate	Na_2HCA	≥0.99	Alfa Aesar	6132-05-4	$C_6H_8Na_2O_7 \cdot 1.5H_2O$	5.24[34] 7.40[34]
Orthophosphoric acid		0.856	VWR	7664-38-2	H_3PO_4	2.89[a][35]
Oxalic acid anhydrous	OA	≥0.99	Fluka	144-62-7	$H_2C_2O_2$	1.98[a][36]
Lignosulphonic acid sodium salt	Na-LS		Sigma-Aldrich	8061-51-6		
Sulphur dioxide				7446-09-5	SO_2	3.40[a][37]
Sulphuric acid solution, 0.25 M		p.a.	Chem-Lab	7664-93-9	H_2SO_4	3.53[b][38]

[a]Only the first dissociation constant is given and was used for calculating the pH value.
[b]Only the second dissociation constant is given. The first proton is assumed to be completely dissociated.

2.2 | Degradation experiments

The furfural degradation experiments were carried out in stainless steel reactors with a volume of approximately 8 ml. A magnetic hotplate stirrer (Heidolph Instruments, Schwabach, Germany) and an aluminium heating block with 12 wells sized to accommodate the reactors were used for agitation and heating. Solutions of furfural and various acids were prepared gravimetrically, 7 ml of which were pipetted into the reactors. The reactors were equipped with a stirring bar, and 11 reactors were placed in the preheated aluminium block simultaneously. Reactions were stirred at 500 rpm, and the temperature of the aluminium block was controlled using a Pt1000 temperature sensor. The actual reaction temperature was measured with another Pt1000 temperature sensor, placed in the remaining 12th well, which accommodated an additional reactor filled with glycerol. At specified time points, the degradation reaction was stopped by removing the reactors and cooling them in an ice bath. Samples were stored in a refrigerator until analyses were carried out. All experiments were performed at least in duplicate.

2.3 | Xylose to furfural conversion experiments

Briefly, 0.1 mol L^{-1} solutions of D-xylose in sulphuric or formic acid were prepared and heated to 150°C using the same experimental setup as for the degradation experiments. To follow the course of the conversion, the reaction was stopped at various time points, and the samples were stored in a refrigerator until further analyses were carried out. All experiments were performed in duplicate.

2.4 | pH measurements and calculations

The pH of the solutions was measured prior to the degradation experiments using a HI1230 pH electrode connected to a HI83141 pH metre (both Hanna Instruments GmbH, Graz, Austria). The pH values at the temperature investigated were calculated from the acid concentration and the temperature dependencies of the various acid dissociation constants K_a given in the literature (see Table 1).

2.5 | HPLC analysis

Chromatographic analysis was performed using a Thermo BDS Hypersil C8 (4.6 mm × 250 mm, 5 μm) analytical column at room temperature and a Dionex P680 isocratic pump operating at a flow rate of 1 ml min^{-1}. Furfural was detected using a Dionex UVD 340 UV detector operating at a wavelength of 277 nm and was quantified by external calibration. An aqueous solution of acetonitrile ($w = 20\%$) was used as an eluent, the sample

volume was 20 µl, and the run time was set to 7.5 min per sample.

2.6 | Ion chromatography analysis

The concentration of formate was determined using a Dionex GS50 equipped with a Kontron 465 autosampler, a Dionex IonPac AS11-HC (4 mm × 50 mm) guard column, and a Dionex IonPac AS11-HC (4 mm × 250 mm) separation column. A Dionex ED 50 conductivity detector with an ASRS Ultra II (4 mm) suppressor was used, and formate was quantified by external calibration. Samples were eluted using a mixture of deionized water (eluent A), 5 mmol L^{-1} of sodium hydroxide (eluent B), and 200 mmol L^{-1} of sodium hydroxide (eluent C) at a flow rate of 1.5 ml min^{-1}. The gradient program is given in Table 2.

TABLE 2 Elution gradient used for the analysis of formate

t (min)	φ (Eluent A)	φ (Eluent B)	φ (Eluent C)
0	0.80	0.20	0.00
8	0.80	0.20	0.00
23	0.65	0.20	0.15
24	0.80	0.20	0.00
30	0.80	0.20	0.00

2.7 | Infrared spectroscopy

Solids from degradation experiments after 300 min were separated by filtration through a polytetrafluoroethylene (PTFE)-filter (Sartorius, 0.45 µm and 47 mm in diameter) and washed with deionized water until neutral pH was achieved; the residue was dried on the filter for 24 h at 40°C and 150 hPa. The solids were analyzed using a Bruker Tensor 27 Fourier-transform infrared (FTIR) spectrometer equipped with a liquid-nitrogen-cooled MCT detector and a Specac single-reflection diamond attenuated total-reflectance (ATR) attachment. Spectra were obtained from 64 scans with a resolution of 2 cm^{-1} in the range of 600–4000 cm^{-1}. All spectra were baseline–corrected, and an average spectrum was calculated.

2.8 | Zeta potential measurements

Solids from degradation experiments after 240 min were suspended in deionized water at a concentration of 1 g L^{-1}. Zeta potentials were analyzed using a Malvern Pananalytical Zetasizer Nano ZSP at 20°C.

2.9 | Scanning electron microscopy (SEM)

A FEI Quanta 450 microscope was used for microscopic investigations. All samples were deposited on adhesive carbon tape and coated with a thin gold film using a Fisions Instruments Polaron SC502 sputter coater.

2.10 | Preparation of lignosulphonic acid (LSA)

A strong cation exchange resin (Amberlite IR120, 49.50 g) was activated in a saturated solution of sodium chloride (100 ml) for 24 h and then treated with a 0.025 g/g (2.5 mass%) solution of sodium hydroxide for 80 min. After washing with distilled water until neutral pH, it was treated with a 0.05 g/g (5 mass%) hydrochloric acid solution for 12 h. The resin was transferred to a column and washed with deionized water until the runoff liquid had a neutral pH. A solution of the sodium salt of LSA (15.03 g) in deionized water (250 ml) was passed through the column at a speed of approximately one drop per minute, and LSA (11.24 g) was obtained as a yellow solid after evaporating and drying the resulting solution.

2.11 | Preparation of sulphurous acid

Sulphurous acid was prepared by introducing SO_2 gas into water. The concentration of SO_2 in the resulting aqueous solution was determined by titration with chloramine-T, using potassium iodide and starch as indicators. A concentration of 99.2 mmol L^{-1} SO_2 was measured.

2.12 | Conversion calculations and kinetic modelling

The conversion of furfural X(FU) was calculated from the initial furfural concentration (FU) and the concentration after the degradation experiments (FU) according to Equation (1):

$$X(\mathrm{FU}) = \frac{[\mathrm{FU_0}] - [\mathrm{FU}]}{[\mathrm{FU_0}]} 100\% \quad (1)$$

For estimating the overall reaction order of furfural in Section 3.1, the initial reaction rates were calculated by

determining the slope of the linear regression for the observed furfural degradation without adding acid catalyst. The slope can be regarded as the initial reaction rate because the conversion for experiments without added acid catalyst was below 32% in any case, and furfural degradation showed linear behaviour during the time investigated with coefficients of determination being higher than 0.98. The detailed calculation can be found in Section S1 in the supporting information.

The selectivity for formic acid $S(\mathrm{FA})$ was calculated by dividing the amount of formed formic acid (FA) by the amount of degraded furfural according to Equation (2):

$$S(\mathrm{FA}) = \frac{[\mathrm{FA}]}{[\mathrm{FU}_0] - [\mathrm{FU}]} 100\% \tag{2}$$

The influence of the initial furfural concentration, furfural conversion, and temperature on the formic acid selectivity was evaluated by fitting selectivity data to a three-factor quadratic model. Furthermore, 48 sets of reaction conditions (see Table S3 in the supporting information) were analyzed using the regression tool in Design Expert statistical software (version 13.0.4.0, Stat-Ease Inc., Minneapolis, MN, USA). Since the experiments do not follow a statistical experimental design, but are based on data from furfural degradation experiments, the validity of the experimental design was evaluated in terms of standard error and Pearson's r correlation matrix. Insignificant model terms ($p < 0.1$) were omitted, and the significance of the obtained model was tested by analysis of the variance (ANOVA). The goodness-of-fit was determined by evaluating the regression coefficient R^2, the adjusted R^2, and the predicted R^2. The model equation, evaluation of the experimental design, and analysis of variance can be found in Section S3 in the supporting information.

The hydrogen ion concentration in the solutions of the various acids at the reaction temperature was calculated using Equation (3), which is derived from the dissociation equilibrium as well as material and ion balances. This can be seen as follows:

$$[\mathrm{H_3O^+}] = -\frac{K_\mathrm{A}(T)}{2} + \sqrt{\left(\frac{K_\mathrm{A}(T)}{2}\right)^2 + K_\mathrm{A}(T) c_0} \tag{3}$$

where $K_\mathrm{A}(T)$ is the acid dissociation constant at the reaction temperature (taken from the literature; see Table 1) and c_0 is the concentration of the acid.

For modelling the degradation kinetics, the rate equations based on the proposed mechanisms were implemented in MATLAB. The recorded concentrations of furfural and formic acid over time at the pH value of the acid catalyst used were employed to estimate the kinetic parameters, that is, rate constants and hydrogen ion concentration exponent. The system of ordinary differential equations was solved numerically using the *ode45* function, and parameter estimation was performed using the *lsqcurvefit* function, which is a non-linear least-squares solver based on the trust-region-reflective algorithm. Considering that the furfural concentrations were 10–100 times higher than the formic acid concentration, statistical weighting was applied to avoid dominance of the furfural concentration during the fitting procedure. The fit quality was monitored by calculating the coefficient of determination and by parity plots.

3 | RESULTS AND DISCUSSION

3.1 | Kinetics of furfural degradation in pure water

Furfural degradation experiments in 0.1 mol L^{-1} solutions of 10 different acids were performed using furfural concentrations of 5, 10, 25, and 50 g L^{-1} at the temperatures of 125, 150, 175, and 200°C. Furfural conversion reached between 10% and 55% after 6 h.

To investigate the overall order of the reaction, experiments without adding acid were conducted at the same four initial furfural concentrations. Figure 1A shows that the conversion of furfural at 150°C decreased with increasing initial concentration, which indicates that the order of furfural degradation is less than one. The opposite was observed at the higher temperature of 200°C (see Figure 1B): with increasing initial furfural concentrations, conversion increases, indicating an order of the furfural degradation greater than one. Estimation of the overall reaction orders via the initial-reaction-rates method gave reaction orders of 0.8 and 1.3 for 150 and 200°C, respectively (see Figure 1C,D). This behaviour indicates the presence of several parallel reaction pathways with reaction rates of similar magnitude but different activation energies. At low temperatures, the overall reaction order was less than one, which indicates a predominant reaction in which furfural is in excess over a second reaction partner. This may be due to reactions catalyzed by the metal surface of the reactor, oxidation reactions, or chain-growth polymerizations. The higher reaction order at increased temperatures suggests that bimolecular reactions, such as condensations, become more favourable. Lamminpää et al.[18] also observed variations in furfural degradation reaction orders, depending on the acidity of the formic acid solution used.

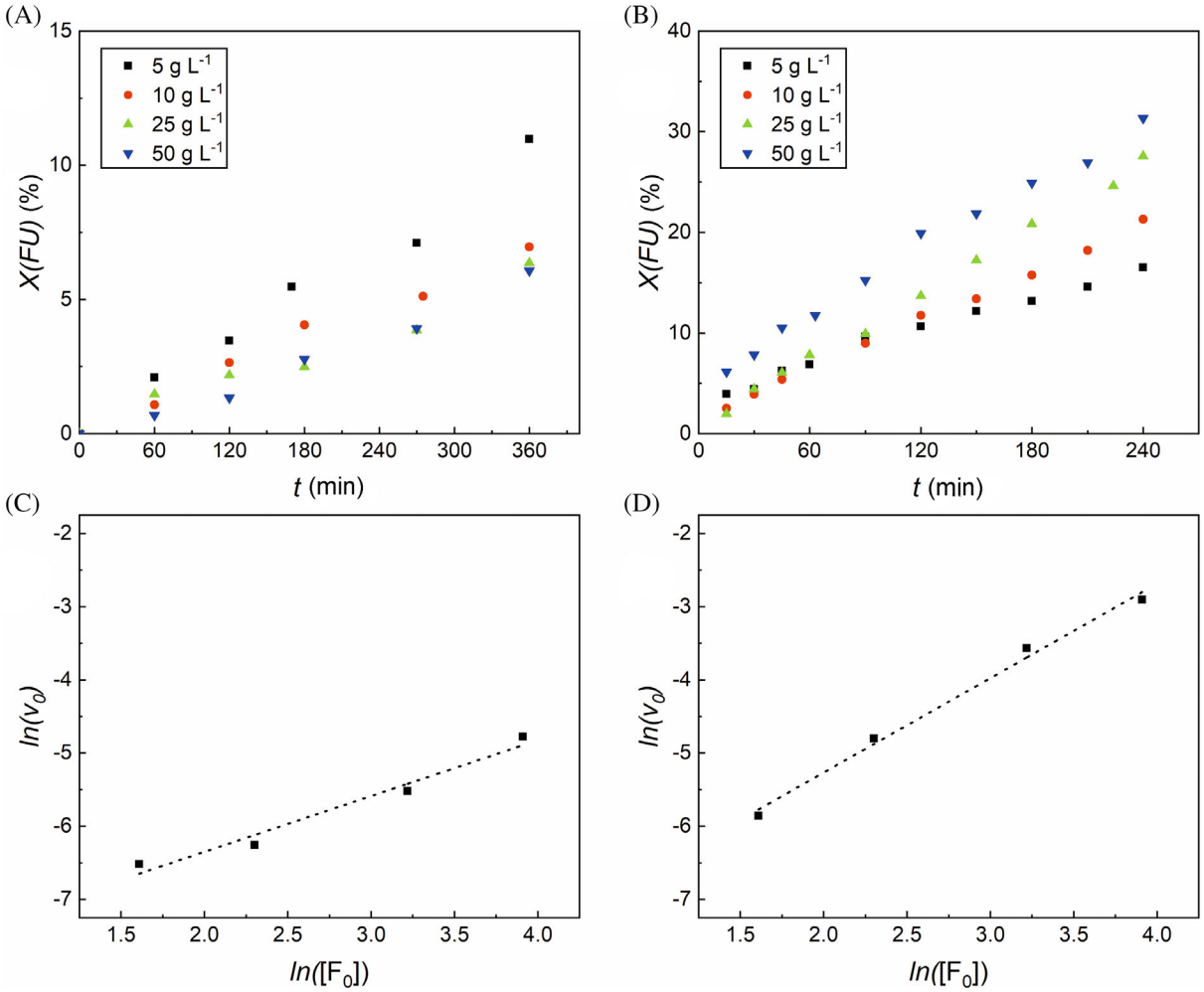

FIGURE 1 Conversion of furfural *X*(FU) in aqueous solutions at various initial concentrations and (A) 150 and (B) 200°C. Plots of the logarithmic initial concentration ln([FU_0]) versus the logarithm of the conversion rate ln(v_0) at (C) 150 and (D) 200°C are used for estimating the overall order of reaction. A detailed calculation of initial reaction rates can be found in the supporting information (Section S2).

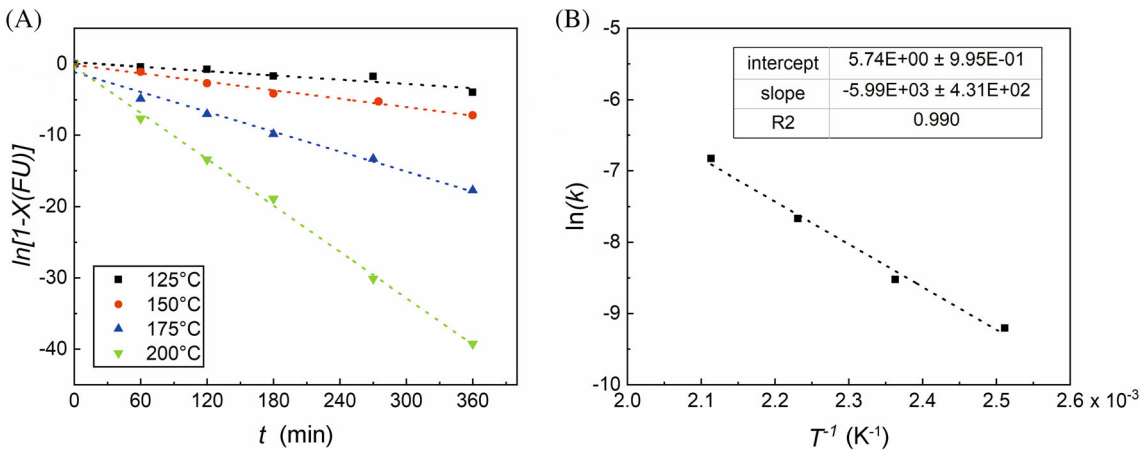

FIGURE 2 (A) Logarithmic plot of the furfural conversion over time at various temperatures and (B) the corresponding Arrhenius plot for determining the overall activation energy of the furfural degradation in water

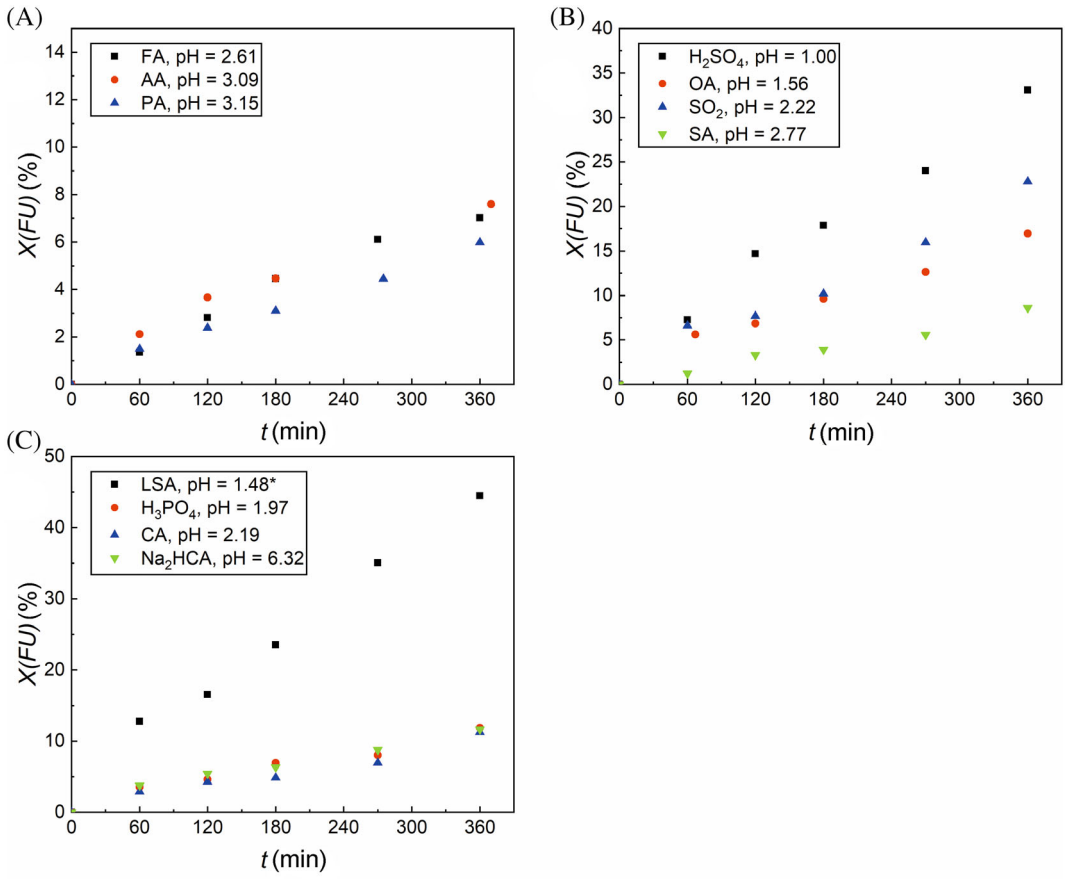

FIGURE 3 Conversions of furfural at 150°C in 0.1 M L^{-1} aqueous solutions of (A) monovalent (formic acid, FA; acetic acid, AA; propionic acid, PA), (B) divalent (sulphuric acid, H_2SO_4; oxalic acid, OA; sulphur dioxide, SO_2; succinic acid, SA), and (C) trivalent acids (lignosulphonic acid, LSA; phosphoric acid, H_3PO_4; citric acid, CA; disodium hydrogen citrate, NA_2HCA). The pH values were calculated for the reaction temperature, and the initial concentration of furfural was 1 mass%. *Given the lack of thermodynamic data for LSA, the pH measured at room temperature was used.

To determine the overall activation energy of the furfural loss reactions, experiments at various reaction temperatures and an initial furfural concentration of 10 g L^{-1} were conducted. Figure 2 shows the conversion of furfural at reaction temperatures between 125 and 200°C. To estimate the overall activation energy, a reaction order of one was assumed. The corresponding Arrhenius plot is shown in Figure 2. An overall activation energy of 49.8 kJ mol^{-1} was calculated, which is in the similar range of published values without an acid catalyst, ranging from 44.2 to 58.8 kJ mol^{-1}. Added acid catalyst values ranging from 48.1 to 110.3 kJ mol^{-1} can be found in the literature.[39]

3.2 | Furfural degradation in various acids is influenced by their acidity and reactivity

Figure 3 shows the experimental data for various mono-, di-, and tri-valent acids at 150°C and an initial concentration of 0.01 g/g (1 mass%) furfural. In general, the conversion of furfural increased with the decreasing pH value of the solution, which is in support of a hydrolytic route of furfural degradation. In Figure 3A, the degradation of furfural in formic acid deviates from this general trend. Although formic acid was the strongest carboxylic acid investigated, the furfural conversion observed in this case was less than for all other monovalent acids. Despite formic acid being known to be unstable under acidic conditions at higher temperatures, chromatographic analysis revealed that its concentration remained constant throughout the reaction. Additional formation of formic acid could not be quantified because due to the high initial concentration, the small amounts originating from furfural degradation were not observable. The reduced furfural degradation in formic acid can therefore be explained by formic acid being formed during furfural breakdown, which leads to a shift of the reaction equilibrium to the educt side. Conversely, the conversion observed for sulphurous acid is higher than

expected based on its pH value. It is known that the aldehyde group of furfural can undergo nucleophilic attack from hydrogensulphite ions, forming bisulphite adducts.[40] This reaction is assumed to be an additional reason for furfural losses.

LSA is a water soluble, acidic polymer and is formed by the acidic cleavage of ether bonds and subsequent sulphonation of lignin. It is a by-product of the sulphite pulping process and could therefore serve as a cheap, biomass-based catalyst for the conversion of hemicellulose to furfural. In addition, spent sulphite liquor is rich in hemicellulose and can therefore be considered as a feedstock for furfural production. However, LSA may not only catalyze the conversion of hemicellulose to furfural, but also further degrade it to undesirable products. For this reason, the interactions between furfural and LSA were investigated and compared to those of furfural with other acids. LSA was prepared from Na-LSA, and the concentration of acidic sites was determined based on by the sulphur content and by titration of a 20 g L^{-1} LSA solution with 0.1 mol L^{-1} NaOH. The results of 2.08 mmol g^{-1} sulphur content and 1.92 mmol g^{-1} acid equivalent determined by titration are in good accordance with values reported in the literature.[41] Figure 3C shows that at a concentration of 0.1 mol L^{-1} acidic groups, which corresponds to a total LSA concentration of 52.1 g L^{-1}, the highest level of furfural degradation for all acids investigated (at equivalent molar concentrations) was observed for LSA. Compared to oxalic acid, which has a similar pH, three times more furfural was degraded in the presence of LSA. This finding explains a previous report of a comparably low yield of 21% for lignosulphonate-catalyzed dehydration of xylose to furfural in ionic liquids.[42] While it is known that sulphur-free lignin may be polymerized by furfural, to the best of our knowledge, this is the first report of a purified lignosulphonate reacting in the same way.[43] Other acids, such as sulphuric, phosphoric, and citric acid, are even stronger but did not exhibit an equally high degradation rate. Thus, if spent sulphite liquor is being considered as raw material for furfural production, lignosulphonates should be completely removed prior to acid hydrolysis.

Aside from the previously mentioned cases, no significant influence of the valency on the acids investigated was observed. Additionally, there was no difference in terms of degradation behaviour between furfural in organic and in inorganic acids. From Figure 3, it can be seen that regardless of the valency or chemical nature of the acid used, furfural conversion is strictly monotonously increasing with decreasing pH value.

To prove that furfural degradation at a given temperature and concentration is only dependent on the pH value, we performed experiments with acetic acid, succinic acid, and phosphoric acid, all at a pH value of 2.5 at 150°C and an initial furfural concentration of 10 g L^{-1}. This corresponds to concentrations of 1.52, 0.344, and 0.011 mol L^{-1} of acetic acid, succinic acid, and phosphoric acid. No significant difference in the conversion of furfural between the three acids was observed, with furfural conversions being 6.23, 6.29, and 6.35 for acetic acid, succinic acid, and phosphoric acid, respectively.

One might argue that acid anions could influence furfural degradation, especially because halides are known to catalyze the dehydration of sugars due to their basic and nucleophilic character, and chloride ions were found to accelerate furfural degradation in aqueous solutions. [44,45] Enslow and coworkers proposed that chloride ions may stabilize oxocarbenium ions, thus promoting the nucleophilic attack on the carbonyl group. However, a catalytic effect of anions, other than chloride has never been described for the degradation of furfural or HMF. Our observation that the rate of conversion increased continuously with proton concentration and the constant conversion with different acids at the same pH value discussed above does not suggest any anion effect for the investigated acids under biorefinery-like conditions. This could be explained by the lower nucleophilicity of the studied carboxylates compared to halides.[46] Further, studies investigating the effect of chloride ions used concentrations of at least 1 mol L^{-1} chloride, as compared to 0.1 mol L^{-1} of acids in our study. Therefore, a significant anion effect under the conditions investigated seems very unlikely.

3.3 | A common set of soluble degradation products is accompanied by acid-specific compounds

To further investigate the reaction pathways of furfural degradation, the reaction solution was analyzed by a gas chromatography with mass spectrometry detector (GC–MS) and ion chromatography after the degradation experiments. Minor amounts of glycolic acid, 2-furoic acid, lactic acid, pyruvic acid, and various C_5 and C_4 hydroxylic acids were detected. Significant amounts of levulinic acid as well as small quantities of furfuryl alcohol were only present in the liquid of the degradation experiment with 0.1 mol L^{-1} H_2SO_4. This may be explained by the hydrogenation of furfural and subsequent degradation of furfuryl alcohol to levulinic acid.[47] Hydrogenation was probably promoted by hydrogen formed from sulphuric acid attacking the steel reactor walls under the conditions investigated.

Formic acid was the most abundant soluble degradation product, as previously reported by others.[48,49] However, its formation over the course of furfural degradation has hitherto not been studied. To increase our understanding of the reaction pathways, we quantified the

formic acid amounts formed at a range of reaction times and under various conditions. As expected, at higher temperatures and higher acidities, formic acid formation increased with increasing furfural degradation. The formic acid amount formed relative to the degraded furfural (i.e., the selectivity) was in the range of 8%–35% and changed depending on the conditions. A higher acidity increased the selectivity of formic acid formation, which suggests that this reaction pathway follows a specific acid catalysis mechanism. In the experiments with sulphuric acid and SO_2, much less formic acid was formed than expected based on the pH values (see Figure 4). In the case of sulphuric acid, this was due to the hydrogenation of furfural to furfuryl alcohol, as mentioned above. As stated earlier, the aldehyde group is suggested to form adducts with hydrogensulphite ions in sulphurous acid solution, which prevents it from being split off by water hydrolysis.[40]

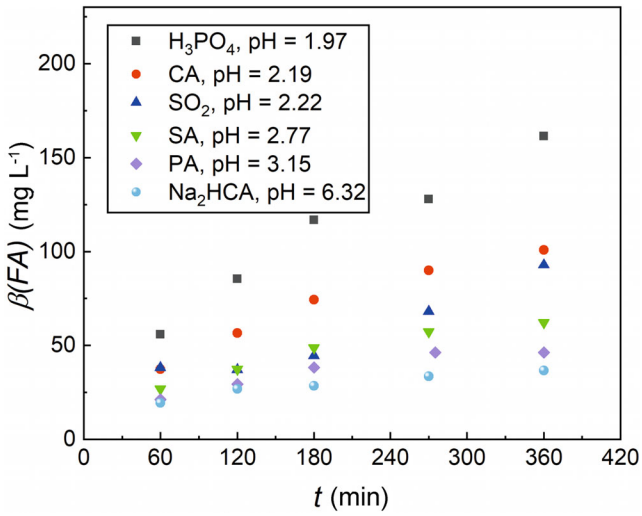

FIGURE 4 Formation of formic acid (FA) during the degradation of a 0.01 g/g (1 mass%) furfural solution at 150°C in various 0.1 M L^{-1} acids (phosphoric acid, H_3PO_4; citric acid, CA; sulphur dioxide SO_2; succinic acid, SA; propionic acid, PA; disodium hydrogen citrate, NA_2HCA)

To show the influence of reaction conditions on formic acid selectivity without acid catalyst graphically, the data were fit to a three factor reduced quadratic model using non-linear regression. The model equation, fit statistics, and analysis of variance can be found in Appendix S1. Figure 5A,B show the selectivity for formic acid as a function of the reaction temperature and furfural conversion at initial furfural concentrations of 10 and 50 g L^{-1}, respectively. For both concentrations, the trends are similar, with formic acid selectivity being generally higher at lower initial furfural concentrations. At high initial concentrations, the selectivity decreases because the probability of bimolecular reactions, such as condensations and aromatic substitutions, increases.

Figure 5A,B shows that the selectivity for formic acid is highest at low conversions of furfural and decreases in the course of furfural degradation. We suggest that the formation of formic acid via hydrolytic ring cleavage of furfural is accompanied by the formation of aliphatic aldehyde species that are more reactive than furfural itself or act as an initiator for further furfural degradation. 2-Oxopentanedial 1 and succinaldehyde 2 (see Scheme 1) are possible hydrolysis products, and unlike furfural, each of these molecules can undergo multiple aldol reactions with other carbonyl species. The reactivity of these species is emphasized by the fact that we did not detect any of these C_4 or C_5 aliphatic aldehydes and only minor amounts of furan during LC–MS and GC–MS analysis. Furthermore, in Sections 3.4 and 3.5, we found

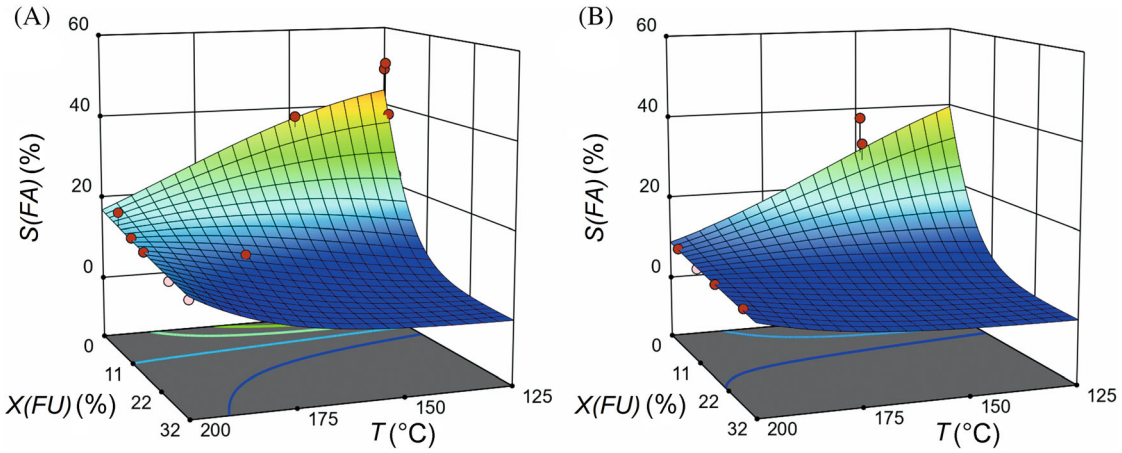

FIGURE 5 Selectivity S(FA) for formic acid formation from furfural as a function of furfural conversion and temperature at initial furfural concentrations of (A) 10 and (B) 50 g L^{-1}. Details on the quadratic model and the analysis of variance can be found in the supporting information (Section S3).

that the same conditions, leading to an increased formic acid selectivity, also promoted particle nucleation, which further supports this theory.

Low temperatures promote the formation of formic acid, especially at low furfural conversions as can be seen in Figure 5. Assuming first-order kinetics, an activation energy for the formic acid pathway of 27.0 kJ mol^{-1} was estimated, which is significantly lower than the estimated value of 49.8 kJ mol^{-1} for the overall reaction (the corresponding Arrhenius plots can be found in Section S4 in the supporting information). As a result, this pathway is dominant at lower temperatures.

A slight increase in formic acid selectivity with increasing temperature is observed at high furfural conversions. However, in the region of low temperature and high conversion, the standard error is high because no data points are present due to time limitations (see Figure S2 in the supporting information).

3.4 | The presence of two orthogonal reaction pathways is supported by infrared spectroscopy findings

ATR-infrared (IR) spectra were recorded to analyze the characteristics of the solid furfural degradation products, called humins. All spectra feature broad, overlapping absorption bands, which indicate a complex, polymeric molecular structure, and are in good agreement with previously reported spectra.[22] A broad absorption band from 2500 to 3700 cm^{-1} with a maximum at around 3300 cm^{-1} found in all samples is attributed to O—H stretching vibrations. Weak contributions of C—H vibrational bands show the presence of furanic (3120–3140 cm^{-1}) and aliphatic (2930 cm^{-1}) structures. The most intense absorptions are the C═O stretch of conjugated carbonyl groups at around 1700 cm^{-1} and the C═C stretch of furanic rings at 1600 cm^{-1}. The bands at 1460 and 1390 cm^{-1} are also ascribed to C═C ring stretches, and the 1020 cm^{-1} band is a characteristic ring deformation vibration of furans. C—H out-of-plane vibrations gave absorptions at 885, 800, and 750 cm^{-1} in the low wavenumber region of the spectrum.[50,51] As the pH value decreased, the ratio of C═O to C═C stretching vibration increased, which can be seen in Figure 6A. At low acidities, the absorption band at 1600 cm^{-1} was dominant, but it decreased, and in experiments with acids stronger than formic acid, the C═O absorption at 1700 cm^{-1} became the most intense band. In addition, the bands at 1460, 1020, and 885 cm^{-1} became less pronounced, while the C—H out-of-plane vibration at 800 cm^{-1} increased. These observations are in accordance with the formation of formic acid at high acidities as described in Section 3.3. Hydrolytic cleavage leads to the formation of formic acid and an enol species, which is subsequently converted to succinic aldehyde. This dialdehyde may undergo further reactions, such as aldol condensations, which lead to cross-linked molecules rich in carbonyl groups. Aldol reactions between aliphatic aldehydes and furfural or recyclization of carbonyls, as well as direct polymerization of two furfural molecules, may lead to aromatic structures, which are responsible for absorptions in the 1000–1500 cm^{-1} range. This explanation is in accordance with the observations of Shi et al.[52] who studied the hydrothermal degradation of carbohydrates and different furans. The authors also found that the formation of aliphatic carbonyl species and subsequent aldol reactions are responsible for the formation of solid humin by-products.

Interestingly, Patil and Lund[24] observed the opposite behaviour for HMF-derived humins, where the intensity of the envelope of peaks in the 1150–1350 cm^{-1} range increased relative to the 1550–1750 cm^{-1} range when acid catalysts were present. They postulate that HMF forms humins via acid-catalyzed hydrolytic ring opening and subsequent aldol reactions. These aldol reactions are thought to decrease the amount of carbonyl groups in the humins formed, whereas most of the furan rings stay intact. Generally, HMF and furfural-derived humins show many similarities, both in their physico-chemical properties, and in the involved mechanisms, with hydrolytic ring cleavage and subsequent aldol reactions being important in both cases. However, IR spectra revealed distinct differences in their formation mechanisms and in the influence of acid catalysts and other reaction conditions. These differences are probably caused by the substitution of the five-position on HMF, which is known to be susceptible for electrophilic additions of carbonyl groups.[53]

When the initial furfural concentration was increased from 10 to 50 g L^{-1} at constant temperature, the maximum of the C═O band shifted to smaller wavenumbers, and the intensity of the C—H out-of-plane vibrations and the furanic C—H stretching vibration increased, which can be seen in Figure 6B. Compared with spectra obtained for stronger acids, this observation indicates a more conjugated structure with more intact furan rings. As can be seen in Figure 6B, the described effect is less pronounced at 200°C.

In conclusion, the infrared analysis shows that at least two different mechanisms lead to the formation of solid degradation products. High acidities promote hydrolytic cleavage of the furan ring, which is accompanied by the formation of formic acid and aliphatic carbonyl groups. These carbonyl groups can undergo aldol-reactions that result in highly branched polymeric structures. Higher furfural concentrations, however, lead to polymerization reactions, such as electrophilic aromatic substitutions in which the furanic structure is preserved. At higher temperatures, the

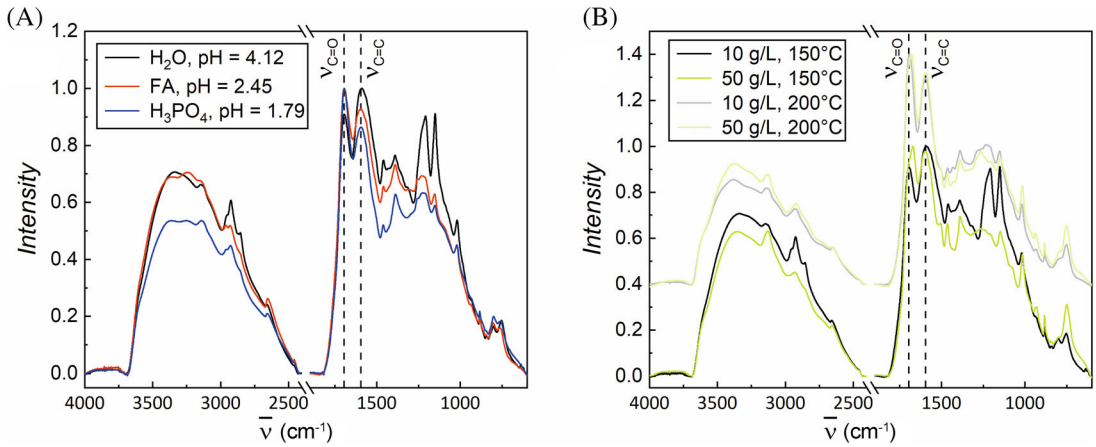

FIGURE 6 Infrared spectra of the solid degradation products of (A) 10 g L^{-1} furfural solutions in water (black), 0.1 M L^{-1} formic acid (FA, red) and 0.1 M L^{-1} phosphoric acid (H_3PO_4, blue) at 150°C. (B) The infrared spectra of the solid degradation products of 10 (black) and 50 g L^{-1} (green) aqueous furfural solutions at 150 and 200°C. Spectra at 200°C were vertically offset by 0.4 units to provide better readability. The two strong bands at 1200 and 1150 cm^{-1} were caused by the PTFE-filter.

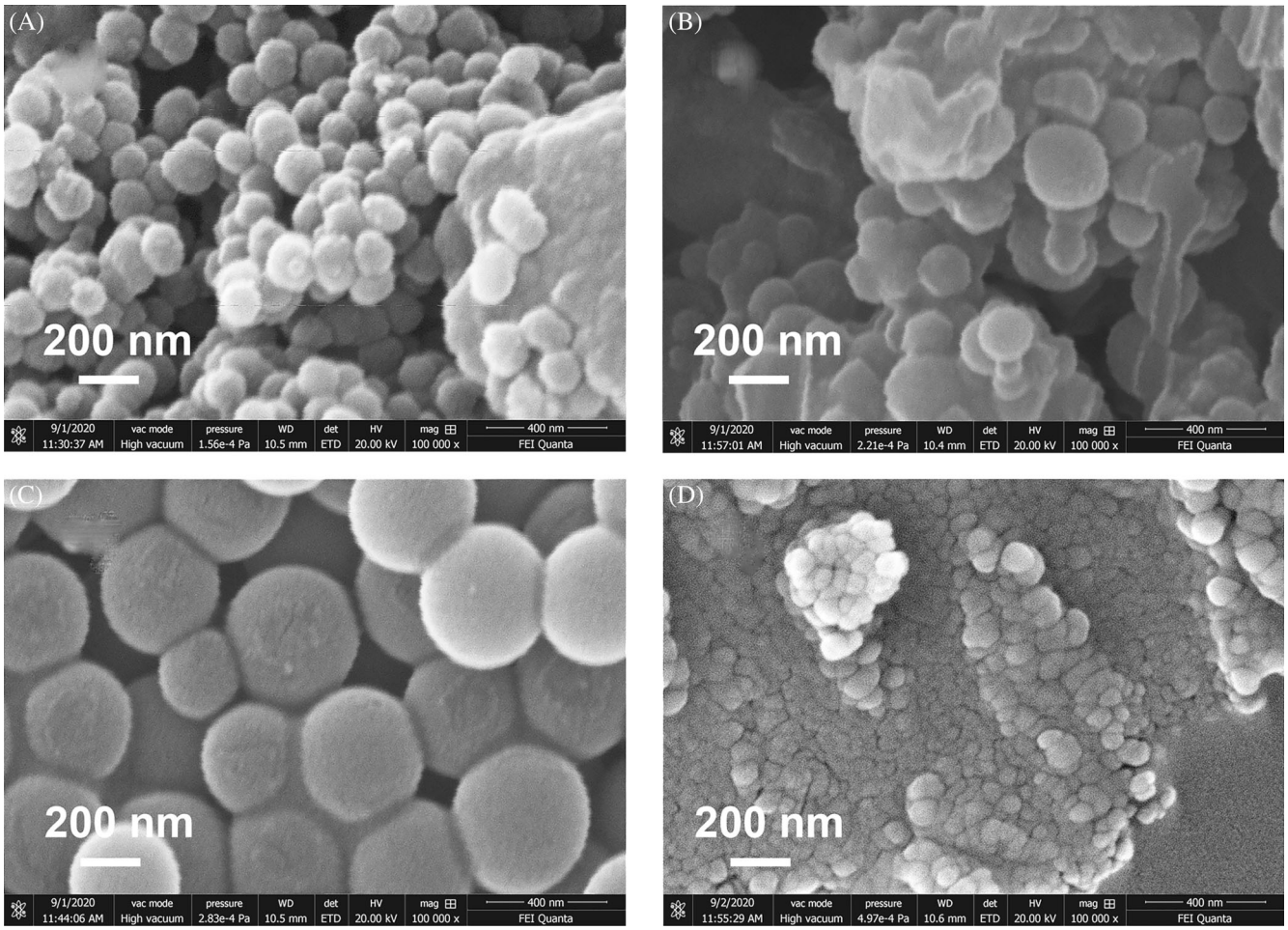

FIGURE 7 Scanning electron microscopy (SEM) images of humins formed during the degradation of (A) 10 g L^{-1} furfural in H_2O at 150°C (7% conversion), (B) 50 g L^{-1} furfural in H_2O at 150°C (6% conversion), (C) 50 g L^{-1} furfural in H_2O at 200°C (5% conversion), and (D) 10 g L^{-1} furfural in 0.1 M L^{-1} formic acid at 150°C (7% conversion)

hydrolytic cleavage is less dominant due to the different activation energies for the formic acid and the direct polymerization pathway (see Section 3.3). As a result, the difference in spectra of 10 and 50 g L^{-1} furfural solutions is less pronounced at higher temperatures, which can be seen in Figure 6B.

3.5 | Morphology of solid degradation products

To investigate the influence of the reaction conditions on the formation of solid degradation products, called humins, SEM images were recorded. The electron micrographs show that, under the conditions investigated, furfural degradation caused spherical particles to form with diameters in the range of 40–500 nm. All electron micrographs show a uniform, monomodal particle size distribution; we can therefore conclude that new-particle formation is faster than particle growth.[21] In general, for a given conversion, particle size increased with increasing temperature and furfural concentration, as can be seen in Figure 7. Interestingly, temperature and furfural concentration seemed to have a greater influence on the particle size than on furfural conversion. When acid catalysts were present (Figure 7D), furfural tended to form smaller humins than in pure water. This finding indicates separate reaction pathways for initial particle formation and for particle growth. Tsilomelekis et al.[21] also described two distinct reaction mechanisms for the formation of humin particles from HMF, and they observed smaller particles without an acid catalyst added. In contrast to their findings, for furfural, we found that particle size decreased with the decreasing pH value of the solution. Given the analysis of the FTIR data in Section 3.4, we postulate that the acid-catalyzed hydration of furfural leads to the nucleation of humins via ring opening and subsequent aldol reactions (see Scheme 1). This is consistent with observations from Section 3.3, where we found high selectivity for hydrolytic ring opening only at the beginning of furfural degradation and no open ring products were found. On the other hand, the uncatalyzed reaction pathway leads to continued particle growth, which involves electrophilic aromatic attack of the carbonyl atom of furfural or Diels–Alder reactions.

The presence of acid catalysts not only led to decreased particle size but also to more interconnections between the humin particles. Zeta potential measurements revealed a potential of −58.9 mV for particles formed from a 50 g L^{-1} aqueous furfural solution and of −53.5 mV for particles formed from a 50 g L^{-1} furfural solution in 0.1 mol L^{-1} formic acid, both kept at 200°C for 4 h. The negative potential is believed to be caused by carboxylic acid groups, which can be formed from α-carbonyl aldehydes via hydration and 1,2-hydride shift, as can be seen in Scheme 1. The proposed condensation product serves as an example that features all structural characteristics that were described in Section 3.4. Under acidic conditions, two effects lead to

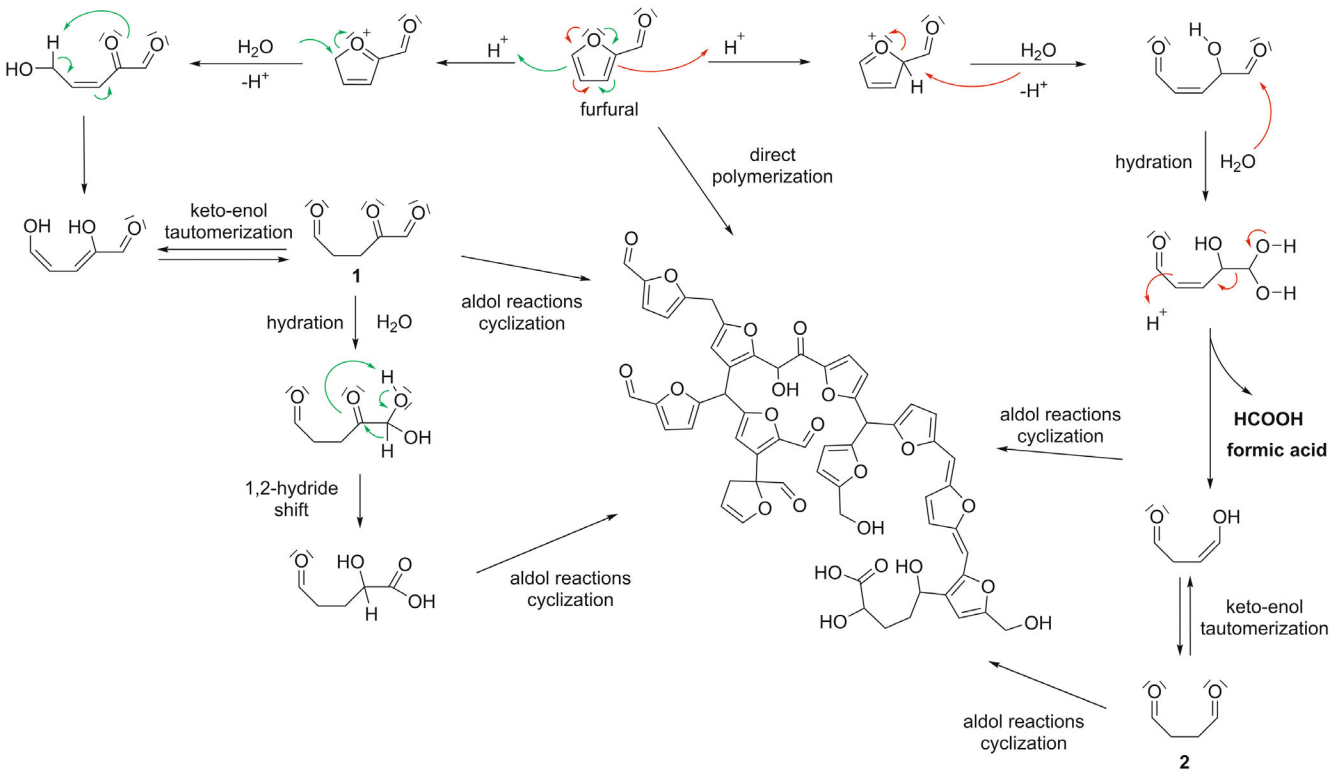

SCHEME 1 Different pathways for the acid catalyzed hydration of furfural showing the formation of formic acid, acidic groups, and the main structural features of furfural condensation products. The coloured arrows indicate the movement of electron pairs for the cases of the proton attacking at C_5 (green) or at C_2 (red).

more interconnected particles: first, the competitive hydrolytic cleavage of formic acid reduces the amount of α-carbonyl aldehydes and thus the formation of acidic surface groups. Second, lower pH causes the acid groups to be protonated, which further reduces the surface charge and leads to the coagulation of the particles.

3.6 | Proposed reaction mechanism and kinetic modelling

The results above suggest that there are multiple furfural degradation pathways. To describe furfural degradation quantitatively, the mechanism from Scheme 1 was simplified to a model consisting of two main degradation pathways. The first includes the formation of formic acid, follows the specific acid catalysis mechanism, and is of first order. As discussed in Section 3.2, this step seems to be reversible, because the addition of formic acid reduced furfural degradation. The second pathway is thought to be a polymerization reaction and is considered to be uncatalyzed and of second order. An aldehyde group may react in an electrophilic aromatic substitution reaction with the free five-position of a furfural molecule. The aldehyde group may originate from furfural or a hydrolysis product thereof. The latter is assumed to be more reactive because in furfural, the conjugated aromatic structure diminishes the electrophilicity of the carbonyl group. Diels–Alder or hetero-Diels–Alder reactions have also been proposed for the polymerization of furfural,[16] although this type of reaction would not retain the furan ring and therefore contradicts the results from our IR-analysis. However, to some extent, these reactions could also occur in parallel to aromatic substitution reactions. The simplified reaction pathways and the corresponding kinetic model based on the findings of this study are shown in Scheme 2.

According to Scheme 2, the reaction rate for the degradation of furfural is given by:

$$\frac{d[\mathrm{FU}]}{dt} = -k_1[\mathrm{FU}]^2 - k_2[\mathrm{H}^+]^h[\mathrm{FU}] + k_2'[\mathrm{H}^+]^h[\mathrm{FA}], \quad (4)$$

where k_1 is the rate constant for the uncatalyzed pathway, and k_2 and k_2' are the rate constants for the formation of formic acid and the back reaction from formic acid, respectively. [FU] is the furfural concentration, [FA] the concentration of formic acid, and $[H^+]$ is the hydrogen ion concentration with the corresponding hydrogen ion concentration exponent h. The hydrogen ion concentration was calculated according to Equation (3) by considering the applied acid catalyst and the amount of formic acid formed. The first term in Equation (4) describes the furfural loss via direct polymerization and

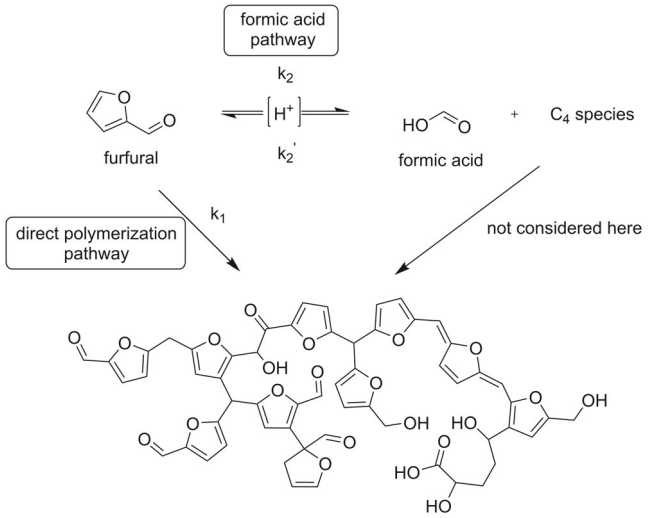

SCHEME 2 Proposed furfural degradation mechanism considering the formation of formic acid

the second term gives the acid-catalyzed furfural degradation to formic acid and further unknown species. The third term describes the back reaction from the formic acid pathway.

For the formation of formic acid, a second rate equation can be formulated as follows:

$$\frac{d[\mathrm{FA}]}{dt} = k_2[\mathrm{H}^+]^h[\mathrm{FU}] - k_2'[\mathrm{H}^+]^h[\mathrm{FA}] \quad (5)$$

The values of the kinetic parameters were estimated by fitting them to the experimental data at 150°C:

$$\frac{d[\mathrm{FU}]}{dt} = -2.2\times10^{-3}[\mathrm{FU}]^2 - 2.6\times10^{-3}[\mathrm{H}^+]^{0.58}[\mathrm{FU}] + 7.3\times10^{-2}[\mathrm{H}^+]^{0.58}[\mathrm{FA}] \quad (6)$$

Sulphuric acid, sulphur dioxide, and LSA were excluded due to specific side reactions, as explained in Sections 3.2 and 3.3. The coefficients of determination (R^2) show that the proposed model fits the experimental data well, as can also be seen in the parity plots in Figure 8. The fit quality is better for the formation of formic acid, which is due to the less precise method used for determining the furfural concentration. When the proton concentration is considered, the higher rate constant for the direct polymerization pathway shows that it is preferred over the acid-catalyzed hydrolytic cleavage at 150°C. As the acidity rises, the formic acid pathway becomes more dominant, and thus the overall reaction order of furfural decreases. At higher temperatures, in contrast, the reaction order increases, as the higher

activation energy of the direct polymerization pathway is overcome more easily.

Figure 9 shows the experimental and modelled data for the conversion of furfural and the formation of formic acid.

3.7 | Conversion of xylose catalyzed by formic acid

To demonstrate how the findings above can be used to optimize furfural production processes, experiments on the acid-catalyzed conversion of xylose to furfural were conducted. The reaction temperature, pH value, and xylose-to-acid ratios were chosen to match the conditions typical of industrial furfural production processes.[9]

As can be seen in Figure 10, under the conditions investigated, nearly 100% of the xylose was converted after 6 h in both acids, as the pH value was the same. Interestingly, xylose conversion was at first faster in sulphuric acid, but the reaction rate declined after 120 min. In formic acid, the reaction rate was lower at the beginning but did not decrease after 120 min, and after 270 min, the conversion of xylose was approximately the same in both acids. The formation rate of furfural from xylose was the same in both acids during the first 3 h of the reaction. At a yield of roughly 40%, the formation rate of furfural catalyzed by H_2SO_4 declined, and a final yield of 45% furfural was achieved. In contrast, the furfural formation rate when catalyzed by formic acid did not decline until a yield of 56% was reached, and the final yield was 57% after 6 h. These findings confirm the

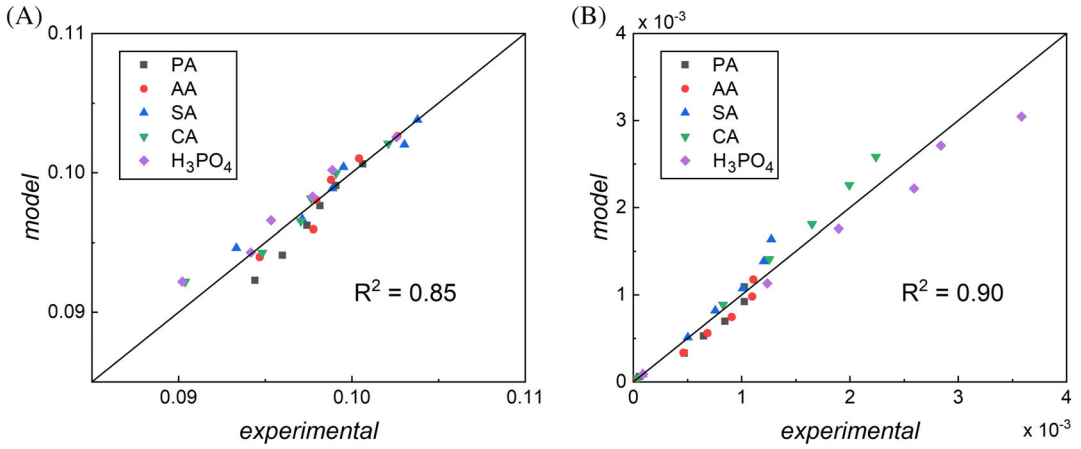

FIGURE 8 Parity plots for (A) the furfural concentration and (B) the formic acid concentration during degradation experiments of 0.01 g/g (1 mass%) furfural solutions at 150°C in various acids (propionic acid, PA; acetic acid, AA; succinic acid, SA; citric acid, CA; phosphoric acid, H_3PO_4)

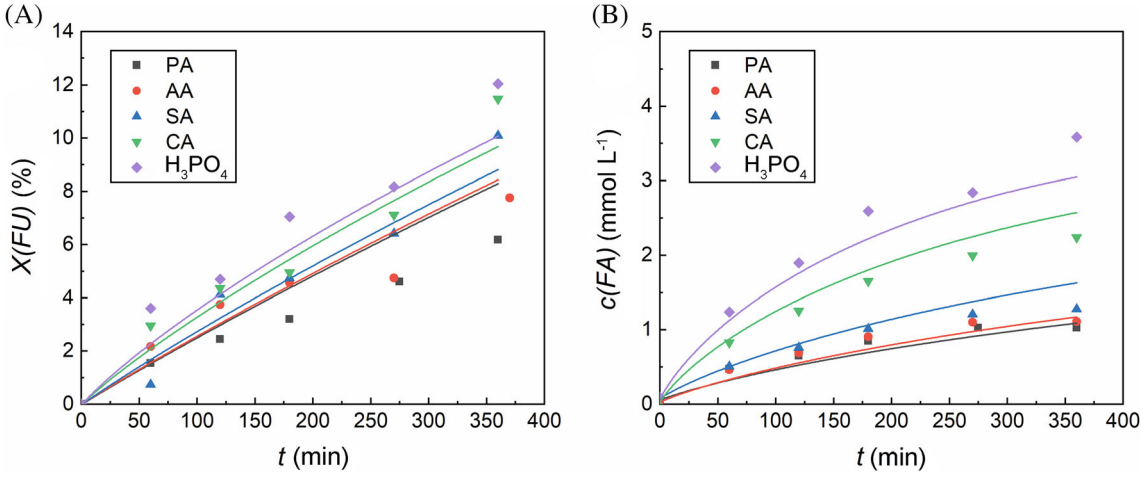

FIGURE 9 Experimental (symbols) and modelled (solid lines) data for (A) furfural degradation and (B) the accompanying formation of formic acid in 0.01 g/g (1 mass%) furfural solutions at 150°C in various acids (propionic acid, PA; acetic acid, AA; succinic acid, SA; citric acid, CA; phosphoric acid, H_3PO_4)

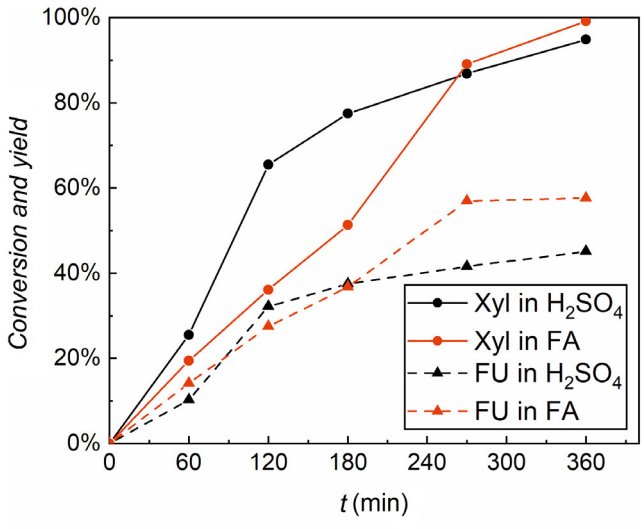

FIGURE 10 Conversion of D-xylose (Xyl, solid lines and circles) and furfural yield (FU, dashed lines and triangles) in 2.5 M L^{-1} formic acid (FA, shown in red) and 0.0125 M L^{-1} H_2SO_4 (shown in black) at 150°C. For both solutions, the pH calculated based on the reaction conditions was 1.9.

results of the kinetic modelling based on the proposed reaction mechanism. According to this mechanism, formic acid suppresses some of the degradation reactions of furfural, while degradation proceeds unhindered in sulphuric acid. Although the xylose conversion rates were different at the beginning of the reaction, the selectivity for furfural was higher in formic acid for each single reaction time. At complete conversion after 6 h, the selectivities for furfural formation from xylose under the conditions investigated and catalyzed by sulphuric and formic acid were 47% and 58%, respectively.

This observation confirms our assumed reaction mechanism and proves that our findings can be applied to optimize the production processes of furfural. When formic acid is used for the production of furfural from hemicellulose-rich feedstocks, a higher yield can be achieved. Consequently, fewer degradation products are formed, which results in reduced fouling problems in the reactor and in the downstream processing units. Formic acid has previously been described as a suitable catalyst for xylose conversion,[54] but its beneficial effects and their causes have not been detailed. In common industrial processes, furfural is continuously removed from the aqueous phase to reduce the amount of undesirable side reactions of furfural. Therefore, the effects described here are expected to be much less pronounced in commercial production units.

Nevertheless, formic acid would be a more eco-friendly alternative to sulphuric acid because it can be produced from biomass via a catalytic oxidation process (OxFA process) or from CO_2 and hydrogen or water.[55] However, these technologies are not yet economically viable, and the higher cost of formic acid compared to sulphuric acid has to be considered. Regarding process safety, the toxicity and flammability of formic acid may be problematic when used in industrial processes.

4 | CONCLUSION

Our study is the first to investigate furfural degradation in 10 different acids of relevance in the biorefinery industry. Our results showed that, in relation to furfural degradation, there are no differences between organic or inorganic acids and that furfural loss does not depend on the acid's valency. For organic acids commonly found in biomass hydrolysates, we observed that the degradation rate was dependent only on temperature, furfural concentration, and hydrogen ion concentration. For acids present in sulphite pulping processes, namely, sulphurous acid and LSA, high degradation rates were observed due to bisulphite and condensation reactions, respectively. Furfural degradation experiments under various conditions, infrared analysis, and investigation of particle morphology suggest multiple pathways for the degradation of furfural. We observed that formic acid formation follows an acid-catalyzed mechanism and that this reaction is reversible. Formic acid may thus slow down the degradation of furfural to some extent. Further, we proposed a kinetic model capable of describing the observed behaviour.

The results presented here show that both LSA and sulphurous acid are not preferred catalysts for furfural production and that their presence in biorefinery feedstocks is detrimental to the production of furfural. The proposed kinetic model serves to predict and explain quantitatively the reactivity of furfural under acidic conditions and could be used to increase furfural yields in industrial processes. More detailed research will be necessary to investigate additional parameters of relevance in industrial streams and side reactions with non-acidic biomass components such as extractives.

NOMENCLATURE

AA	acetic acid
ATR	attenuated total reflection
CAS Reg. No.	Chemical Abstracts Service Registry Number
CA	citric acid
c	molar concentration (mol L^{-1})
FA	formic acid
FTIR	Fourier-transform infrared
FU	furfural
GC–MS	gas chromatography with mass spectrometry detector

HMF	5-hydroxymethylfurfural
IR	infrared
k	reaction rate constant
K_A	acid dissociation constant
LC-MS	liquid chromatography with mass spectrometry detector
LSA	lignosulphonic acid
MCT	mercury cadmium telluride
Na_2HCA	disodium hydrogen citrate
Na-LS	lignosulphonic acid sodium salt
OA	oxalic acid
PA	propionic acid
PTFE	polytetrafluoroethylene
R^2	coefficient of determination
SA	succinic acid
SEM	scanning electron microscopy
t	time (s)
UV	ultraviolet
v_0	initial reaction rate (mol min^{-1})
X	conversion
Xyl	D-(+)-xylose

Greek letters

$\tilde{\nu}$	wavenumber (m^{-1})

AUTHOR CONTRIBUTIONS

Lukas Almhofer: Formal analysis; investigation; writing – original draft; writing – review and editing. **Robert H. Bischof:** Project administration; writing – review and editing. **Martin Madera:** Conceptualization; resources. **Christian Paulik:** Supervision; writing – review and editing.

ACKNOWLEDGEMENTS

We would like to acknowledge the Austrian government, the provinces of Lower Austria, Upper Austria, and Carinthia, as well as Lenzing AG, for financial support. Also, we would like to express our gratitude to the Johannes Kepler University, Linz; the University of Natural Resources and Life Sciences (BOKU), Vienna; and Lenzing AG for their in-kind contributions.

Furthermore, we would like to thank colleagues from Wood K + Daniela Bammer and Markus Huemer, as well as Klaus Schlackl, Sebastian Schönauer, Erwin Malzner, Walter Milacher, and their teams from Lenzing AG for the extraordinary support in the laboratories of Lenzing AG.

FUNDING INFORMATION

This work was supported by the Austrian Research Promotion Agency (FFG) (grant number: 844608).

DATA AVAILABILITY STATEMENT

The data that support the findings of this study are available from the corresponding author upon reasonable request.

ORCID

Lukas Almhofer https://orcid.org/0000-0003-4810-3642

REFERENCES

[1] International Advisory Council of GBS2018, Commoniqué Global Bioeconomy Summit 2018, https://gbs2018.com/fileadmin/gbs2018/Downloads/GBS_2018_Communique.pdf (accessed: April 2021).
[2] Top Value Added Chemicals from Biomass (DOE/GO-102004-1992), https://www.osti.gov/biblio/15008859-top-value-added-chemicals-from-biomass-volume-results-screening-potential-candidates-from-sugars-synthesis-gas (accessed: December 2021).
[3] J. J. Bozell, G. R. Petersen, *Green Chem.* **2010**, *12*, 539.
[4] X. Li, R. Xu, J. Yang, S. Nie, D. Liu, Y. Liu, C. Si, *Ind. Crops Prod.* **2019**, *130*, 184.
[5] Z. Zhang, *ChemSusChem* **2016**, *9*, 156.
[6] J.-P. Lange, E. van der Heide, J. van Buijtenen, R. Price, *ChemSusChem* **2012**, *5*, 150.
[7] R. Mariscal, P. Maireles-Torres, M. Ojeda, I. Sádaba, M. López Granados, *Energy Environ. Sci.* **2016**, *9*, 1144.
[8] G. Marcotullio, *Ph.D. Thesis*, Delft University of Technology, Delft, The Netherlands **2011**.
[9] K. J. Zeitsch, *The Chemistry and Technology of Furfural and its Many By-Products*, Elsevier, Amsterdam, The Netherlands **2000**.
[10] J. van Buijtenen, J.-P. Lange, L. Espinosa Alonso, W. Spiering, R. F. Polmans, R. J. Haan, *ChemSusChem* **2013**, *6*, 2132.
[11] C. H. J. T. Dietz, M. Verra, S. Verberkt, F. Gallucci, M. C. Kroon, M. F. Neira D'Angelo, M. Papaioannou, M. van Sint Annaland, *Ind. Eng. Chem. Res.* **2019**, *58*, 16116.
[12] G. Gómez Millán, S. Hellsten, A. W. T. King, J.-P. Pokki, J. Llorca, H. Sixta, *J. Ind. Eng. Chem.* **2019**, *72*, 354.
[13] X. Hu, R. J. M. Westerhof, L. Wu, D. Dong, C.-Z. Li, *Green Chem.* **2015**, *17*, 219.
[14] S. Peleteiro, S. Rivas, J. L. Alonso, V. Santos, J. C. Parajó, *Bioresour. Technol.* **2016**, *202*, 181.
[15] H. Rasmussen, H. R. Sørensen, A. S. Meyer, *Carbohydr. Res.* **2014**, *385*, 45.
[16] B. Danon, L. van der Aa, W. de Jong, *Carbohydr. Res.* **2013**, *375*, 145.
[17] B. Danon, G. Marcotullio, W. de Jong, *Green Chem.* **2014**, *16*, 39.
[18] K. Lamminpää, J. Ahola, J. Tanskanen, *RSC Adv.* **2014**, *4*, 60243.
[19] I. C. Rose, N. Epstein, A. P. Watkinson, *Ind. Eng. Chem. Res.* **2000**, *39*, 843.
[20] Z. Cheng, J. L. Everhart, G. Tsilomelekis, V. Nikolakis, B. Saha, D. G. Vlachos, *Green Chem.* **2018**, *20*, 997.
[21] G. Tsilomelekis, M. J. Orella, Z. Lin, Z. Cheng, W. Zheng, V. Nikolakis, D. G. Vlachos, *Green Chem.* **1983**, *2016*, 18.
[22] I. van Zandvoort, Y. Wang, C. B. Rasrendra, E. R. H. van Eck, P. C. A. Bruijnincx, H. J. Heeres, B. M. Weckhuysen, *ChemSusChem* **2013**, *6*, 1745.
[23] I. V. Sumerskii, S. M. Krutov, M. Y. Zarubin, *Russ. J. Appl. Chem.* **2010**, *83*, 320.
[24] S. K. R. Patil, C. R. F. Lund, *Energy Fuels* **2011**, *25*, 4745.
[25] N. Shi, Q. Liu, R. Ju, X. He, Y. Zhang, S. Tang, L. Ma, *ACS Omega* **2019**, *4*, 7330.
[26] D. L. Williams, A. P. Dunlop, *Ind. Eng. Chem.* **1948**, *40*, 185.
[27] M. Papaioannou, R. J. T. Kleijwegt, J. van der Schaaf, M. F. Neira d'Angelo, *Ind. Eng. Chem. Res.* **2019**, *58*, 16106.

[28] D. W. Rackemann, J. P. Bartley, W. O. S. Doherty, *Ind. Crops Prod.* **2014**, *52*, 46.
[29] W. Hongsiri, B. Danon, W. de Jong, *Int. J. Energy Environ. Eng.* **2015**, *6*, 21.
[30] Z. Chen, W. Zhang, J. Xu, P. Li, *Chin. J. Chem. Eng.* **2015**, *23*, 659.
[31] V. Majer, J. Sedlbauer, L. Hnedkovsky, R. H. Wood, *Phys. Chem. Chem. Phys.* **2000**, *2*, 2907.
[32] R. E. Mesmer, C. S. Patterson, R. H. Busey, H. F. Holmes, *J. Phys. Chem.* **1989**, *93*, 7483.
[33] R. M. Kettler, D. A. Palmer, D. J. Wesolowski, *J. Solution Chem.* **1995**, *24*, 65.
[34] R. G. Bates, G. D. Pinching, *J. Am. Chem. Soc.* **1949**, *71*, 1274.
[35] K. Ballerat-Busserolles, J. Sedlbauer, V. Majer, *J. Phys. Chem. B* **2007**, *111*, 181.
[36] R. M. Kettler, D. J. Wesolowski, D. A. Palmer, *J. Chem. Eng. Data* **1998**, *43*, 337.
[37] S. A. Rydholm, *Pulping Processes*, Interscience Publishers, New York **1965**.
[38] W. L. Marshall, E. V. Jones, *J. Phys. Chem.* **1966**, *70*, 4028.
[39] J. Köchermann, J. Mühlenberg, M. Klemm, *Ind. Eng. Chem. Res.* **2018**, *57*, 14417.
[40] L. C. Schroeter, *Sulfur Dioxide: Applications in Foods, Beverages, and Pharmaceuticals*, 1st ed., Pergamon Press Inc., Oxford **1966**.
[41] W. Chen, X.-W. Peng, L.-X. Zhong, Y. Li, R.-C. Sun, *ACS Sustainable Chem. Eng.* **2015**, *3*, 1366.
[42] C. Wu, W. Chen, L. Zhong, X. Peng, R. Sun, J. Fang, S. Zheng, *J. Agric. Food Chem.* **2014**, *62*, 7430.
[43] P. Dongre, M. Driscoll, T. Amidon, B. Bujanovic, *Energies* **2015**, *8*, 7897.
[44] W. Guo, H. C. Bruining, H. J. Heeres, J. Yue, *AIChE J.* **2022**, *68*, 17606.
[45] K. R. Enslow, A. T. Bell, *ChemCatChem* **2015**, *7*, 479.
[46] H. Mayr, A. R. Ofial, *Acc. Chem. Res.* **2016**, *49*, 952.
[47] E. I. Gürbüz, S. G. Wettstein, J. A. Dumesic, *ChemSusChem* **2012**, *5*, 383.
[48] B. Cheng, X. Wang, Q. Lin, X. Zhang, L. Meng, R.-C. Sun, F. Xin, J. Ren, *J. Agric. Food Chem.* **2018**, *66*, 11981.
[49] A. P. Dunlop, *Ind. Eng. Chem.* **1948**, *40*, 204.
[50] G. Socrates, *Infrared and Raman Characteristic Group Frequencies: Tables and Charts*, 3rd ed., John Wiley & Sons Ltd., Chichester, UK **2001**.
[51] G. Socrates, in *Infrared and Raman Spectroscopy* (Ed: P. Larkin), Elsevier, Amsterdam, The Netherlands **2018** Ch.6.
[52] N. Shi, Q. Liu, H. Cen, R. Ju, X. He, L. Ma, *Biomass Convers. Biorefin.* **2019**, *10*, 277.
[53] A. Gandini, M. N. Belgacem, *Prog. Polym. Sci.* **1997**, *22*, 1203.
[54] W. Yang, P. Li, D. Bo, H. Chang, *Carbohydr. Res.* **2012**, *357*, 53.
[55] J. Reichert, J. Albert, *ACS Sustainable Chem. Eng.* **2017**, *5*, 7383.

SUPPORTING INFORMATION

Additional supporting information can be found online in the Supporting Information section at the end of this article.

How to cite this article: L. Almhofer, R. H. Bischof, M. Madera, C. Paulik, *Can. J. Chem. Eng.* **2023**, *101*(4), 2033. https://doi.org/10.1002/cjce.24593